Structure of Human Hyaluronidase-1, a Hyaluronan Hydrolyzing Enzyme Involved in Tumor Growth and Angiogenesis[†,‡]

Kinlin L. Chao, Lavanya Muthukumar, and Osnat Herzberg*

Center for Advanced Research in Biotechnology, University of Maryland Biotechnology Institute, Rockville, Maryland 20850

Received February 24, 2007; Revised Manuscript Received April 4, 2007

ABSTRACT: Mammalian hyaluronidases hydrolyze hyaluronan, a polysaccharide of diverse physiological roles found in all tissues and body fluids. In addition to its function in normal cellular hyaluronan turnover, human hyaluronidase-1 is implicated in cancer proliferation, angiogenesis, and inflammatory diseases; its expression is up-regulated in advanced stages of bladder cancer, whereas the expression of the alternative splice-variants is down-regulated. The crystal structure reveals a molecule composed of two closely associated domains: a catalytic domain that adopts a distorted $(\beta/\alpha)_8$ barrel resembling that of bee venom hyaluronidase, and a novel, EGF-like domain, characteristic of involvement in protein−protein interactions and regulatory processes. The structure shows that the fold of this unique EGF-like domain is intact in four alternative splice-variants, whereas the catalytic domain is likely to be unfolded. Thus, these variants may function by competing with the full-length enzyme for the putative protein partner and regulating enzymatic activity in healthy cells.

Hyaluronan (HA[1]) is a linear, unsulfated, negatively charged, glycosaminoglycan formed from ∼2000−25000 repeating disaccharide units of D-glucuronic acid (GlcUA) and *N*-acetyl-D-glucosamine (GlcNAc) with [GlcUA-(β1→3)-GlcNAc-(β1→4)]$_n$ linkages. HA is the major component of cartilage and serves as a joint lubricant. It controls water homeostasis in tissues and the extracellular matrix, which affects cell motility and the distribution and transport of plasma proteins. HA is also implicated in cell proliferation, differentiation, cell−cell recognition, tumor growth and invasion, angiogenesis, and inflammatory responses (*1*−*3*). The cellular role of HA and the HA-mediated signal transduction pathways depends on its size (recently reviewed by Stern et al. (*4*)). Large HA polymers function in organizing the extracellular matrix and serve as lubricant and shock absorber. In shock, septicemia, post surgery, blood loss, and burns, the level of circulating high molecular mass HA increases. These HA polymers are antiangiogenic, immunosuppressive, and anti-inflammatory. In contrast, HA fragments of intermediate sizes are involved in the body's alarm system. They stimulate angiogenesis and inflammatory reactions and facilitate cancer progression and invasion (*4*). Such HA fragments activate several cytoplasmic and extracellular signal transduction pathways associated with Raf-1 kinase, MAP kinase, and ERK. Short HA oligosaccharides are antiapoptotic and inducers of heat shock proteins. They regulate a different set of signaling molecules than the intermediate size HA including Erb2, PTEN phosphatase, and PI 3 kinase (*4*).

Mammalian hyaluronidases are *endo*-β-*N*-acetyl-hexosaminidases (EC 3.2.1.35; glycosyl hydrolase family 56 (*5*)) that hydrolyze the β1→4 glycosidic bond of HA into various oligosaccharide lengths, the shortest of which are tetrasaccharides (*6*). There are five homologous hyaluronidases encoded in the human genome: hHyal-1 through -4 and the sperm adhesion molecule 1 (termed PH-20). In addition, the human genome contains a related pseudo gene, *PHYAL1*. These genes exhibit different tissue distribution profiles. Human Hyal-1 and Hyal-2 are expressed in most tissues and are responsible for the catabolism of intracellular and extracellular HA, respectively (*6*, *7*). With the exception of hHyal-1, the expressed hyaluronidases contain glycosylphosphatidylinositol-signal sequences and are membrane-bound upon maturation. Aside from its primary hydrolytic function, hHyal-2 also serves as a receptor for sheep retrovirus associated with lung cancers, and activates the growth and invasion of brain tumors (*8*−*10*). Human Hyal-3 is expressed in several tissues including the brain, yet its enzymatic activity and biological role are not well-defined. Human Hyal-4 was reported to be specific for chondroitin and chondroitin sulfate substrates (*6*). PH-20 functions during fertilization. It degrades the HA-enriched cumulus of the oocyte during sperm penetration and then serves as the receptor for the sperm binding to the zona pellucida and induces HA-associated sperm signaling.

Human Hyal-1 is a lysosomal enzyme responsible for the hydrolysis of intracellular HA and is also detected in the plasma and in urine (*11*). Increased expression of *HYAL1* mRNA and higher levels of hHyal-1 are documented in many diseases, and in bladder and prostate cancers. The enzyme

[†] Grant sponsors: National Institutes of Health Grant PO1-GM057890. The Advanced Photon Source is supported by the U.S. Department of Energy, Basic Energy Sciences, Office of Science, under Contract W-31-109-Eng-38.

[‡] The coordinates have been deposited in the Protein Data Bank (entry code 2PE4).

* Corresponding author. Mailing address: Center for Advanced Research in Biotechnology, University of Maryland Biotechnology Institute, 9600 Gudelsky Drive, Rockville, MD 20850. Tel: 240-314-6245. Fax: 240-314-6255. E-mail: osnat@carb.nist.gov.

[1] Abbreviations: hHyal, human hyaluronidase; bvHyal, bee venom hyaluronidase; HA, hyaluronan; EGF, epidermal growth factor.

10.1021/bi700382g CCC: $37.00
Published on Web 05/16/2007

is responsible for the production of angiogenic HA fragments. Because of its presence in urine and change in expression level in bladder and prostate cancers, the use of hHyal-1 as a marker of these diseases has been considered (*12*−*14*). Inactivating mutations of hHyal-1 are linked to the human genetic disorder mucopolysaccharidosis IX, characterized by diminished stature, periarticular soft tissue masses, and absence of neurological and visceral involvement (*15*). The plasma HA concentration of patients with this disorder is 40−90-fold higher than in normal serum. The role of hHyal-1 in tumor progression depends on its cellular concentration; it functions as a tumor suppressor at low or very high concentration and as a tumor promoter at moderate concentration (*13*, *16*−*18*).

In humans, eight alternative splice transcripts of *HYAL1* encode the full-length enzyme and five splice variants (*19*). Variants 1−5 (designated v1 through v5) are each truncated to a different extent. They lack enzymatic activity and are expressed at higher level in normal and in grade 1 bladder tumor tissues than in advanced cancer. For example, hHyal-1 v1 expression is 2.3-fold higher in normal bladder tissues than in bladder tumors (*20*), and hHyal-1 v5 is the main transcript in normal bladder cells (*19*). By comparison, the full-length hHyal-1 is expressed at lower level in normal tissues and at elevated levels in grade 2/grade 3 bladder tumors and in invasive tumor cells. Expression of splice variant v1 slows down bladder tumor growth, invasion, and angiogenesis by inducing the cellular apoptosis pathway (*20*).

Human Hyal-1 is a 435 amino acid residue protein exhibiting a narrow acidic pH activity (3−4.5) (*21*), consistent with the low pH in the lysosome. The protein contains 10 cysteines, three predicted N-glycosylation sites, and an N-terminal endoplasmic reticulum signal sequence. It cleaves HA substrates of all sizes into short chains, down to tetrasaccharides. The N-terminal 325 amino acid residues exhibit 31% sequence identity with bee venom hyaluronidase (bvHyal), whose structure has been determined in complex with a HA tetrasaccharide (*22*). The sequence homology implies that this hHyal-1 region adopts the same overall fold as that of bvHyal, comprising a distorted $(\beta/\alpha)_8$ barrel. No sequence homology has been reported in the scientific literature for the C-terminal domains of the mammalian hyaluronidases. However, this region contains a cysteine-rich pattern, $x_4Cx_{0-48}Cx_{3-12}Cx_{1-70}Cx_{1-6}Cx_2Gax_{0-21}Gx_2C$, where "a" denotes a hydrophobic residue, "x" denotes any residue, and the gaps between cysteine residues vary in length as indicated by the subscripts. This pattern is identified in the SMART (*23*) and PROSITE (*24*) databases as an epidermal growth factor (EGF)-like motif.

In vitro biochemical studies of mammalian hyaluronidases have been hampered by the difficulties to produce the enzymes in soluble form. We have overcome this problem by producing recombinant hHyal-1 in *Drosophila* cells. Here we report the crystal structure of the enzyme showing that it contains an EGF-like domain not seen previously, and examine the impact of alternative splicing on the enzyme structure and function.

MATERIALS AND METHODS

Cloning, Expression, and Protein Purification The hHyal-1 gene was amplified from a cDNA clone (MGC-45987, ATCC) and ligated into the *Bgl*II/*Age*I digested pMT/BiP/V5-HisA vector (Invitrogen). The recombinant gene comprises the entire hHyal-1 coding region (Phe22−Trp435) along with two N-terminal amino acids, Arg20 and Ser21, and eight C-terminal amino acids, Thr436, Gly437, and His438−His443 (only Arg20, Ser21, and Thr436 are seen in the electron density map) arising from the cloning procedure. Protein was secreted from stably transfected *Drosophila melanogaster* Schneider 2 cells cotransfected with pCoPuro for selection with puromycin. Protein expression in the conditioned serum-free medium was detected by Western blot analysis with the monoclonal Penta-His Antibody (Qiagen). For large scale expression, stable Schneider 2 cells were grown in shaker flasks at 28 °C and induced with the addition of 0.6 mM $CuSO_4$. The cells were removed by centrifugation after 4 days, and the medium was applied directly onto a Chelating Sepharose Fast Flow column (GE Health Sciences). The protein was eluted with 50−100 mM imidazole and further purified with Sephacryl S200 size exclusion chromatography (GE Health Sciences). The buffer was exchanged with 25 mM sodium acetate at pH 4.6. Protein concentration was determined using the BioRad Protein Assay in conjunction with spectrophotometric measurements (calculated extinction coefficient of 112,120 M^{-1} cm^{-1}). The expression in the *Drosophila melanogaster* Schneider 2 cells yielded ~7 mg of purified protein per 1 L of medium. The molecular mass was measured on a matrix-assisted laser desorption time-of-flight (MALDI-TOF) spectrometer. The N-terminal amino acid sequence was determined as RSFRGPLLP, in accordance with the cloned gene.

Crystallization, Data Collection, and Structure Determination. Crystals were obtained at room temperature by the hanging drop vapor diffusion method. Equal volumes of 10 mg/mL hHyal-1 were mixed with mother liquor containing 1.5 M NaCl, 10% (v/v) ethanol, and 1/10 volume of 30% (w/v) galactose. The drops were equilibrated against the mother liquor reservoir. For data collection, the crystals were transferred to mother liquor supplemented with 30% (v/v) glycerol and flash-cooled at 100 K in liquid propane cooled by liquid nitrogen. Diffraction data were collected at the Southeast Regional-Collaborative Access Team (SER-CAT) 22-BM beamline at the Advanced Photon Source (Argonne National Laboratory, Argonne, IL), which was equipped with a MAR CCD-225 detector. Data were processed with the d*TREK programs (*25*) (Table 1). The structure was determined by molecular replacement with the computer program PHASER (*26*) using the structure of bvHyal as the search model (PDB entry code 1FCU (*22*)). The rotation function *Z*-score was 4.8 and was followed by a translation function *Z*-score of 9.6, indicative of an unambiguous solution. The resulting electron density map revealed locations where side chains of the search model needed to be replaced by the correct side chains of hHyal-1. Building of the HyalEGF-like domain and adjustments to the model were made on a graphics workstation using the program O (*27*). Structure refinement was carried out with the CNS program followed by REFMAC (*28*−*30*). De novo building of the C-terminal domain (83 amino acid residues) was accomplished gradually as the model improved. Water, acetate, and glycerol molecules were added to the model using peaks in the $F_o - F_c$ difference Fourier map with electron density $>3\sigma$ as the acceptance criterion.

Table 1: Data Collection and Refinement Statistics

data collection	
space group	$P3_221$
cell dimensions (Å)	a = *b* = 92.1, *c* = 143.8
resolution (Å)	2.0
wavelength (Å)	1.0000
no. of molecules in the asymmetric unit	1
no. of observed reflections	502,770
no. of unique reflections	47,955
completeness (%)	99.4 (97.7)[a]
multiplicity	10.5 (8.7)[a]
R_{merge}[b]	0.063 (0.488)[a]
$\langle I/\sigma \rangle$	14.0 (3.4)
solvent content	63%
refinement statistics	
resolution range (Å)	80−2.0
total no. of reflections	47,955
completeness	99.4
R_{factor}/R_{free}[b]	0.190/0.230
no. of protein atoms	3280
no. of water molecules	335
no. of sugar units	8
no. of acetate ions	7
no. of glycerol molecules	1
rmsd from ideal geometry	
bond length (Å)	0.019
bond angles (deg)	1.9
average temperature factor (Å)^2	34

[a] The values in parentheses are for the highest resolution shell, 2.07−2.00 Å. [b] $R_{merge} = \sum_{hkl}[(\sum_j|I_j - \langle I\rangle|)/\sum_j|I_j|]$. $R_{factor} = \sum_{hkl}||F_o| - |F_c||/\sum_{hkl}|F_o|$, where F_o and F_c are the observed and calculated structure factors, respectively. R_{free} is computed for 5% randomly selected reflections that were omitted from the refinement.

RESULTS

Overall Structure. Human Hyal-1 was readily crystallized at pH 4.6, within the pH range of enzyme activity. Structure refinement at 2.0 Å resolution (Table 1) yielded a high quality electron density map (Figure 1) covering the entire coding region of the mature hHyal-1 (Phe22−Trp435). All backbone torsion angles are within the allowed regions of the Ramachandran plot.

The hHyal-1 molecule comprises two closely associated domains: the N-terminal catalytic domain (Phe22−Thr352) and the smaller C-terminal domain (Ser353−Trp435) (Figure 2A and B). The catalytic domain adapts a distorted $(\beta/\alpha)_8$-barrel fold similar to that of the bvHyal structure (*22*) but with some variations (Figure 2C): The hHyal-1 β2-strand is missing in bvHyal. However, this β2 does not form β-sheet interactions with β3, hence the β-barrel is open despite the presence of all eight strands. The barrel imperfection extends to the α-helix following β2, which is absent in hHyal-1. A number of secondary structure units are inserted in loops on the C-terminal side of the β-barrel: an α-helix (labeled α4′ following the numbering of the primary β/α motifs), two 3_{10} helices (η4′ and η8′), and a β-hairpin (β3′-3″) (Figures 2B and 3). Two of the five hHyal-1 disulfide bonds (Cys43−Cys333 and Cys207−Cys221) reside in the catalytic domain and are also present in bvHyal (Figure 2C).

The 83-residue C-terminal domain begins with an extension of the catalytic domain's α8 and contains three disulfide bonds. In addition to the helical extension, the domain contains another helix (αI), a reverse turn β-hairpin (βII−βIII), a long two-stranded antiparallel β-sheet (βI and βIV), and a meandering chain at the C-terminus (Figure 2D). The three disulfide bonds are stacked in the order C1−C3, C2−C4, and C5−C6 (Cys358−Cys369, Cys363−Cys418, and Cys420−Cys429), forming the signature pattern of EGF-like domains identified in the SMART (*23*) and PROSITE (*24*) databases. In agreement with this finding, a search of the Protein Data Bank using DALI (*31*) identified the extracellular fragment of the heparin-binding EGF-like growth factor as the closest structural homologue of the hHyal-1 C-terminal domain (*32*), albeit with a low *Z*-score of 2.4 and covering only 38 amino acid pairs (Figure 2D). The aligned residues exhibit 26% sequence identity, and their Cα atoms can be superimposed with root-mean-square deviation of 2.9 Å. The common framework spans the N- and C-terminal two-stranded antiparallel β-sheet (βI−βIV) and the C-terminal coil. Instead of the N-terminal helix present in the EGF-like domain of hHyal-1 (the α8 extension), the heparin-binding growth factor contains an extended polypeptide chain. The EGF-like fold of hHyal-1 is distinguished by a long insertion between the βI and βIV of the EGF core fold, which spans an extended chain followed by a β-hairpin (βII−βIII) and an α-helix (αI) (Figure 2D). Sequence alignment (Figure 3) shows that all other hyaluronidases contain the same structural domain; thus we term it a HyalEGF-like domain.

The HyalEGF-like fold does not resemble the Hyal-1 C-terminal domain fold predicted by ab initio approaches (*33*). The close interaction between the two domains is also very different from the earlier prediction that proposed a flexible linker and lack of interactions between the two domains. Moreover, the modeling of the five human hyaluronidases C-terminal domains yielded a different fold in each case, whereas we expect that these domains adopt the HyalEGF-like fold because the amino acid sequences contain the characteristic disulfide bond pattern.

Protein Glycosylation. The hHyal-1 molecular mass determined by MALDI-TOF mass spectrometry is 50,874 ± 126 Da instead of the calculated molecular mass of 47,368 Da. The mass difference of 3506 Da arises from post-translational N-linked glycosylation. The amino acid sequence of hHyal-1 contains three predicted N-glycosylation sites at Asn99, Asn216, and Asn350; thus the estimated average sugar mass is 1169 Da per site. This is in agreement with previously reported biantennary carbohydrates linked to proteins expressed in *Drosophila* cells (*34*, *35*). $FucMan_3GlcNAc_2$, $Man_6GlcNAc_2$, $FucMan_4GlcNAc_2$, $Man_3GlcNAc_2$, and $Man_3GlcNAc_3$ were the major carbohydrates in glycosylated glutamate carboxypeptidase II expressed in *Drosophila* Schneider 2 cells (*34*). The electron density map of hHyal-1 indicated that all three potential glycosylation sites were modified. The Asn350 modification was the largest seen and was modeled by the branched oligosaccharide:

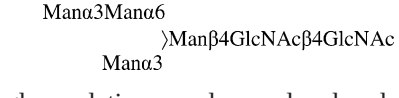

Asn99 N-glycosylation was less ordered and was modeled by $GlcNAc_2$. The oligosaccharide moieties of Asn99 and Asn350 form an intermolecular contact in the crystal. The most solvent exposed Asn216 was associated with weak electron density, which prevented modeling of sugar moieties. The uniform protein glycosylation indicated by the mass spectrometry measurement implies that each oligosaccharide contains an additional mannose or fucose unit beyond

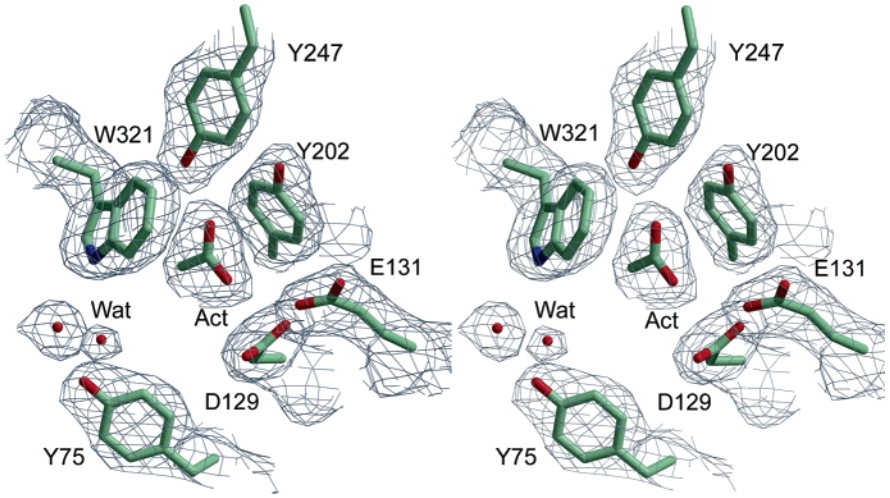

FIGURE 1: Stereoscopic representation of the electron density map in the region of the active site together with the corresponding protein model. The difference Fourier map with sigma(a)-weighted $2F_o - F_c$ coefficients and calculated phases is contoured at 1σ level. "Act" denotes acetate ion and "Wat" water molecule. Atomic color scheme is used: gray, carbon; red, oxygen; blue, nitrogen.

the sugar composition seen in the electron density map linked to Asn350. The Asn350 glycosylation signature sequence is invariant in all mammalian hyaluronidases (Figure 3). This oligosaccharide is located at an interface between the catalytic and the HyalEGF-like module (Figure 2A,B). The oligosaccharide modifications may assist with protein folding and stability, and may play a functional role. Along this line, it was recently reported that treatment of hHyal-1 with N-glycosidase F removed oligosaccharides from 50% of the sample and resulted in 40% reduction of activity (*36*). Human Hyal-1 from bladder tumors has a different N-glycosylation pattern and a slightly different pH activity profile than that of hHyal-1 from normal serum and urine (*37*).

Active Site. As with bvHyal, the active site of hHyal-1 spans an elongated cleft located at the C-terminal end of the α/β-barrel's β-strands (Figure 2). Superposition of the structures of hHyal-1 and the bvHyal-$(GlcUA\text{-}GlcNAc)_2$ complex (*22*) shows that the active site clefts are similar in size and shape (Figure 2C). Many of the active site residues are conserved (Figure 4A), indicating that the mode of tetrasaccharide binding seen in bvHyal is likely to be similar in hHyal-1. Briefly, the cleft is enriched with aromatic residues, characteristic of sugar binding proteins (Tyr75, Trp141, Tyr202, Tyr208, Tyr210, Tyr247, Tyr261, Tyr286, Trp321). There are two arginine side chains that may interact with the carboxylic groups of HA (Arg134, Arg265) and an invariant serine residue (Ser245) that supports the placement of the Tyr202 hydroxyl group. Two invariant acidic residues (Asp129, Glu131) share a proton (Figures 1 and 4A), a recurring catalytic motif not only in the structures of the two hyaluronidases but also in those of glycosyl hydrolases belonging to families 18 and 20 (*38*). An acetate ion (originating from the crystallization solution) is located close to the carboxylate pair and to the Tyr247 hydroxyl, in the same site where the C2 *N*-acetyl group of the tetrasaccharide cleavage product binds to bvHyal. In bvHyal, the position of the *N*-acetyl's oxygen atom is fixed by hydrogen bond interactions (the oxygen atom with Tyr227 hydroxyl group and the NH group with Asp111 carboxyl group) and the methyl group is anchored between aromatic rings (Tyr265, Trp301, and Tyr184). Similarly, one oxygen atom of the hHyal-1 acetate ion is hydrogen bonded to Tyr247 hydroxyl and the acetate's methyl group is tucked between Tyr286, Trp321, and Tyr202. There is a slight difference between the two arrangements because the hHyal-1 Asp129 side chain rotates away from the second oxygen atom of the acetate ion, equivalent to the *N*-acetyl's NH group (Figure 4).

As proposed earlier (*22*), the catalytic mechanism of the hyaluronidases (glycosyl hydrolase family 56) resembles that of the glycosyl hydrolases belonging to families 18 and 20, which involves double displacement at C1 next to the β-(1→4) glycosidic bond to be cleaved. The double displacement results in retention of configuration at C1 (*39*, *40*). Tews et al. proposed a substrate assisted mechanism for the chitin degrading enzymes in which the C2 *N*-acetyl's oxygen atom acts as a nucleophile (*38*). Concomitant with cleavage of the glycosidic bond, a glutamic acid residue (Glu131 in hHyal-1) transfers a proton to the C4 oxygen of the leaving HA fragment. Next, an incoming water molecule replaces the leaving HA fragment. The disposition of active site residues in hHyal-1 suggests that Glu131 and Tyr202 polarize the water molecule for the nucleophilic attack on C1, thus completing the hydrolysis.

Glu268 mutation into a lysine in hHyal-1 is associated with the mucopolysaccharide IX lysosomal storage disorder (*15*). As noted previously (*22*), Glu268 is located remotely from the active site cleft (Figure 4), yet this residue is conserved in all human hyaluronidases. Its side chain is partially buried, forming a hydrogen bond with Asn229 (located on α5) and a salt bridge with Arg271 (located on α6), both invariant residues in the human hyaluronidases. Replacement of this glutamic acid by a glutamine residue in hPH-20 led to loss of activity (*41*). The deleterious effect of a mutation in this position is expected to arise from reduced protein stability due to removal of the electrostatic interaction between α5 and α6.

DISCUSSION

Active Site Specificity. Human hyaluronidases exhibit 33−42% sequence identities and even higher conservation of active site residues. Yet, the enzymes differ in their catalytic efficiencies and pH profiles (*42*). For example, bovine PH-20 (61% sequence identity to the human counterpart) is

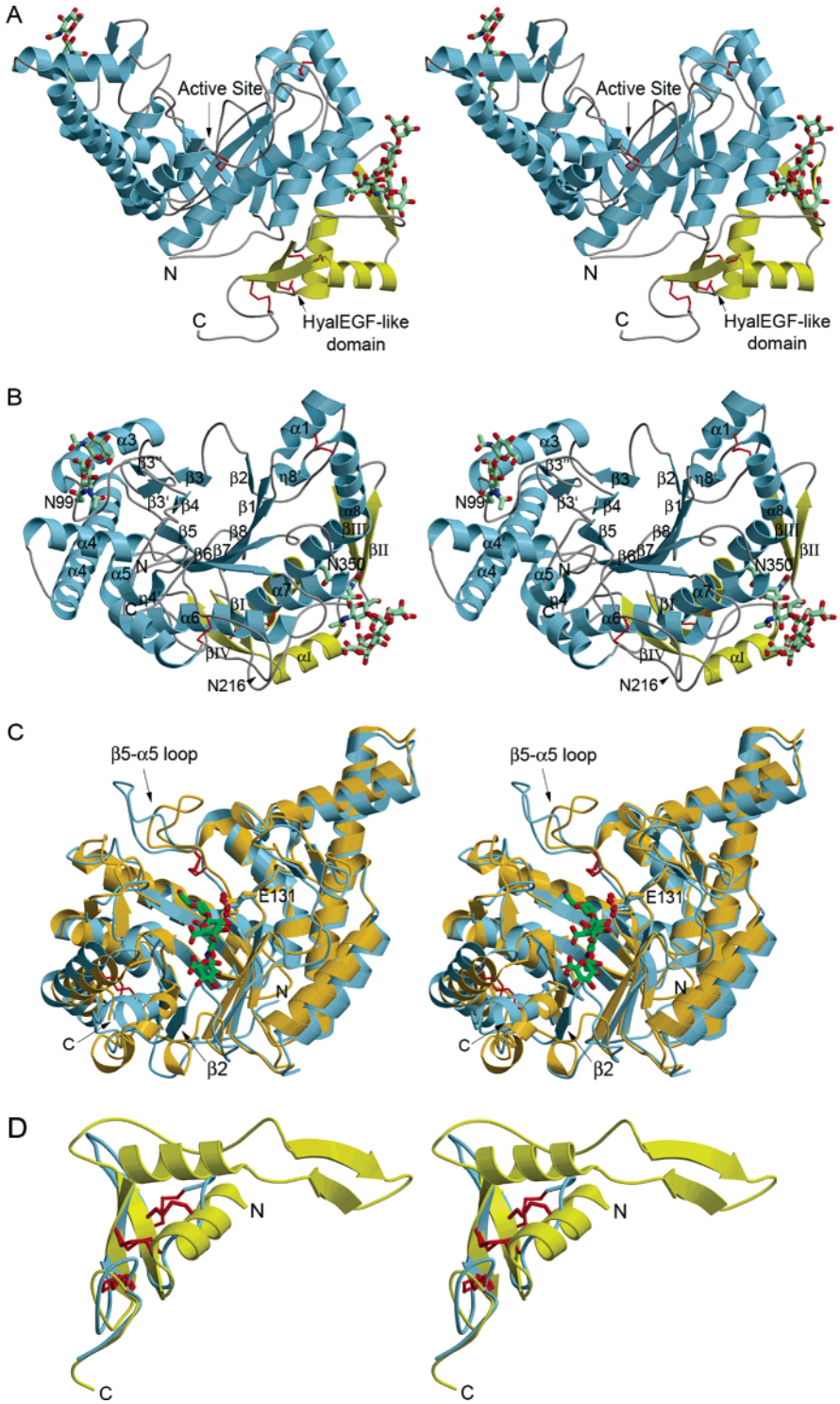

FIGURE 2: Structure of hHyal-1. (A) Stereoscopic representation of a side view. The catalytic and the HyalEGF-like domains are colored light blue and yellow, respectively. Disulfide bonds are shown in red. The N-linked oligosaccharides are shown as stick models with the atomic color scheme: gray, carbon; red, oxygen; blue, nitrogen. (B) A view down the α/β-barrel. The color scheme is as in panel A. Labels of secondary structure units correspond to the labels in Figure 3. (C) Stereoscopic representation of the catalytic domain (colored light blue) superimposed on the structures bvHyal in complex with $(GlcUA\text{-}GlcNAc)_2$ (colored gold; (*22*), PDB entry code 1FCV). The tetrasaccharide is colored with an atomic color scheme: green, carbon; red, oxygen; blue, nitrogen. (D) Stereoscopic representation of the C-terminal domain (colored yellow) superposed on the heparin-binding EGF-like growth factor (colored light blue; (*32*), PDB entry code 1XDT). The disulfide bonds are shown in red.

~400-fold more active than hHyal-2 at acidic conditions (*43*). Human Hyal-1 hydrolyzes HA in a size-independent manner to tetrasaccharides, whereas hHyal-2 specifically degrades large HA polymers into 20 kDa fragments (*44*). The hHyal-1 activity optimum is at pH 3.8, hHyal-2 at pH 5.6−7.0 (*21*, *43*, *44*), and the bovine PH-20 pH profile is bimodal, with maxima at 4.5 and 7.5 (*21*). While the sequences of the reaction centers are conserved in all family members, residues at the peripheries of the active site clefts are more divergent. In particular, the loop connecting β5 and α5 varies

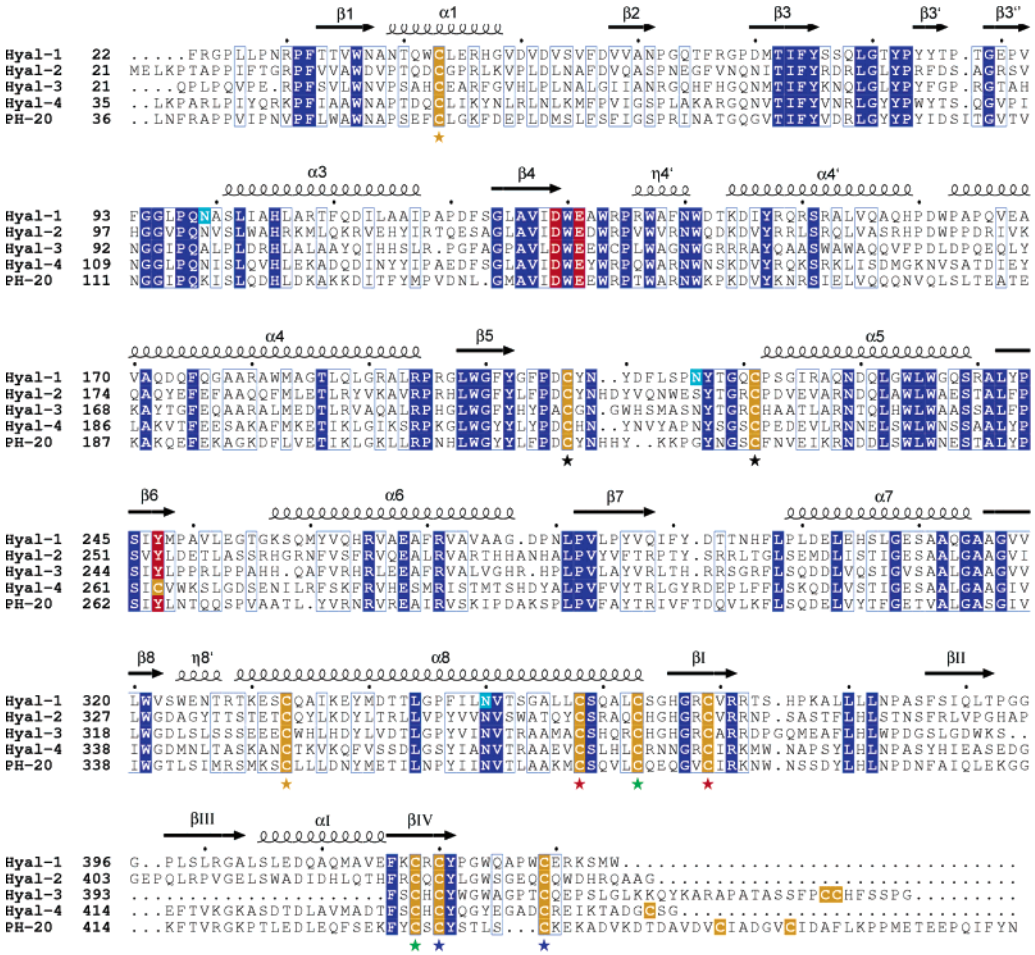

FIGURE 3: Structure-based sequence alignment of human hyaluronidases. Invariant residues are shown in blue except for three key catalytic residues that are colored red. Cysteine residues are colored yellow. The hHyal-1 N-glycosylated asparagines residues are colored turquoise. Residues exhibiting conservative replacements are blocked in blue. Pairs of cysteine residues that form disulfide bonds are indicated by stars with matching colors. Secondary structure units are labeled as in Figure 2B.

in length, composition, and potential glycosylation (Figure 3). Indeed, this loop exhibits a different conformation in hHyal-1 compared with bvHyal (Figure 2C). Such variations may be responsible for the different catalytic properties of the human hyaluronidases. By comparison, the primary substrates of hHyal-4 were reported to be chondroitin and chondroitin sulfate (*6*), which differ from HA in the anomeric form of the C4 hydroxyl of the *N*-acetyl-D-glucosamine unit. We note that hHyal-4 contains a cysteine residue instead of Tyr247, which is the only departure from the conserved catalytic machinery of the hyaluronidases. This change may contribute to the apparent different substrate specificity of hHyal-4.

Role of the HyalEGF-like Domain. All mammalian hyaluronidases contain a C-terminal domain with the same disulfide bond pattern as that observed for hHyal-1. Hence, all are expected to contain the HyalEGF-like domain. The longer hHyal-3 and hPH-20 polypeptides contain two additional cysteine residues which do not align with one another and are not part of the EGF disulfide bond signature sequence (Figure 3). In hHyal-1, the EGF-like domain is located remotely from the active site (over 30 Å away), and thus is not likely to be involved in substrate recognition (Figure 4B). What then is the role of this domain?

Many extracellular proteins contain EGF domains and are involved in cell adhesion and cell−cell communication (*45*, *46*). In the blood coagulation system, the interactions between protease clotting factors are mediated by their EGF domains. Another enzyme, prostaglandin H_2 synthase-1 (cyclooxygenase-1), and its close homologue prostaglandin H_2 synthase-2 (cyclooxygenase-2) also contain an EGF-like domain (*47*). The exact role of the EGF domains is yet to be determined in many cases, but they are thought to mediate protein−protein interactions often associated with regulation of growth and development. Studies have shown involvement of protein partners with hyaluronidases, although the sites of interactions have not been established. The most direct evidence for such interaction pertains to mammalian PH-20, where it was demonstrated that the C-terminal domain encompassing the HyalEGF-like region is responsible for the secondary binding of the acrosome-reacted sperm to the zona pellucida (a glycoprotein membrane) of oocyte during fertilization (*48*). Harada and Takahashi reported that hHyal-1 and hHyal-2 require the HA receptor, CD44, for hyaluronidase activity in vivo and hHyal-2 also requires CD44 for its activity in cell-free solution (*44*). A direct interaction between hHyal-2 and CD44 in the presence of the Na^+-H^+ Exchanger mediates HA-induced cell signaling in human breast tumor cells (*49*). It is tempting to speculate that CD44 may present the HA substrate to the active site of hHyal-1 or hHyal-2 via its interaction with the HyalEGF-like domain. Similarly, it was recently shown that enzymatically inactive mutants of

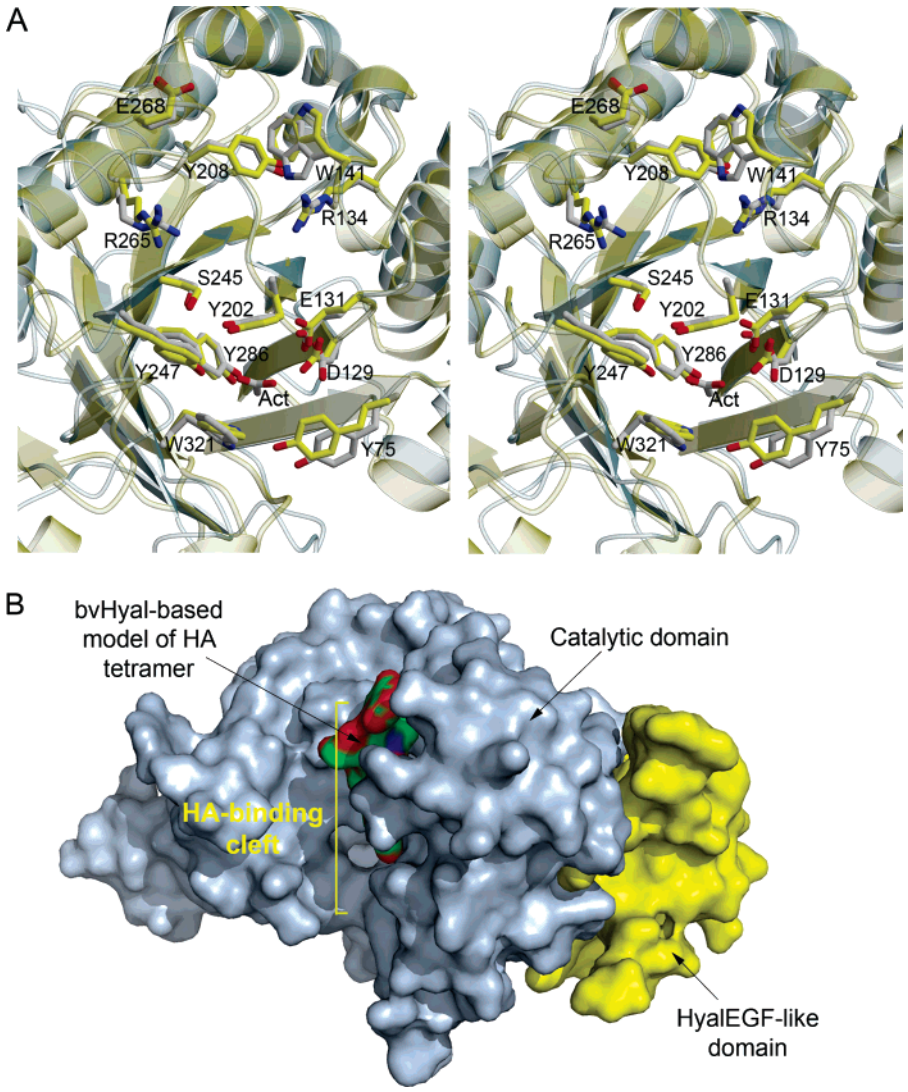

FIGURE 4: (A) Stereoscopic representation of the active site region of hHyal-1 (gray ribbon) superimposed on that of bvHyal (yellow ribbon; (*22*)). Selected amino acids are colored in the atomic color scheme: red, oxygen; blue, nitrogen; gray (hHyal-1) and yellow (bvHyal), carbon. (B) Molecular surface of the catalytic domain (light blue) and HyalEGF-like (yellow) domains of hHyal-1, illustrating the separation between the HyalEGF-like domain and the active site. A docked tetrasaccharide, inferred from the structure of bvHyal, is shown as a space filling model.

hHyal-2 can still serve as the cell-entry receptors of Jaagsiekte sheep retrovirus. These mutations were distributed throughout the catalytic domain and none was located on the HyalEGF-like domain. Hyaluronan did not block the interaction between the viral envelope glycoprotein and hHyal-2; neither did it block the virus infection (*43*). Whether the hHyal-2 HyalEGF-like domain serves as the interaction site for the viral envelope glycoprotein remains to be determined.

The HyalEGF-like domain is elongated and has extensive solvent accessibility, consistent with mediation of protein−protein interactions. The β-hairpin unit (βII−βIII) appears suitable for that role because its flexibility implies potential to adjust in response to a protein partner. Because the sequence of the β-hairpin region varies significantly within the hyaluronidase family (Figure 3), the partner identity or affinity may vary for each enzyme. Now that the 3D structure of hHyal-1 has revealed the presence of a novel HyalEGF-like domain, a search for partners and characterization of their interactions are timely.

Alternative Splicing in hHyal-1. Alternative splicing of hHyal-1 and hHyal-3 have been identified in bladder and prostate cancer cell lines, tumor tissues, and normal kidney tissue, with the two enzymes exhibiting similar splicing patterns (*19*, *50*). The levels of normal and splice variant mRNAs vary in different stages of tumor progression (*19*). In vitro translated splice variants of hHyal-1 (v1 through v5) lack enzymatic activity, consistent with the structure that shows that the deletions destroy the fold integrity of the catalytic domain. Even for the shortest deletion of hHyal-1 v1 (and also hHyal-3 v1), the thirty amino acids comprising the α7, β8, and η8′ units are deleted (Figure 5). Mapping the deletions on the structure of hHyal-1 reveals that the v1, v2, v4, and v5 splice variants retain the HyalEGF-like domain, whereas v3 lacks the HyalEGF-like domain as well as part of the catalytic domain (Figure 5). Notably, the hHyal-1 v5 splice variant comprising solely the HyalEGF-like domain is the major hHyal-1 transcript found in normal bladder, G1 bladder tumor tissues, and normal bladder primary culture, whereas the full-length enzyme dominates in advanced stages of bladder cancer (*19*). In contrast, the

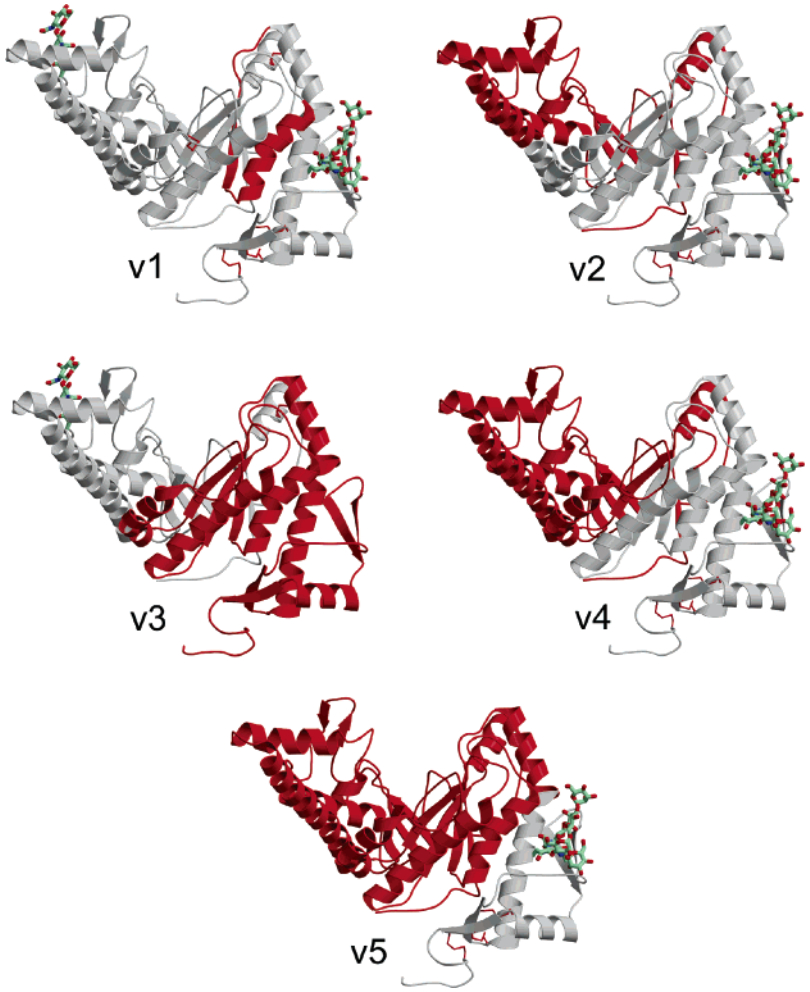

FIGURE 5: Mapping of hHyal-1 splice variants (numbered v1 to v5) on the intact structure. Deleted segments are highlighted in red.

hHyal-3 v3 splice variant, encompassing mainly the HyalEGF-like domain, is the major transcript in all bladder tumor cells and tissues and in prostate cancer cells (*19*).

The three disulfide bonds of the HyalEGF-like domain may help maintain its fold even when the catalytic domain unfolds. Therefore, hHyal-1 splice variants in which the HyalEGF-like domain remains intact may have regulatory roles by binding to the partner protein and modulating the enzymatic activity of the full-length enzyme. An alternative regulatory mechanism was recently suggested by Lokeshwar and colleagues, who showed by immunoprecipitation experiments that the hHyal-1 v1 splice variant forms a complex with the full-length hHyal-1, resulting in 4-fold inhibition of hyaluronidase activity and reduced production of angiogenic HA fragments (*20*). Their studies also showed that overexpression of the hHyal-1 v1 splice variant activated the apoptosis pathway in HT1376 bladder cancer cells and slowed bladder tumor growth, invasion, and angiogenesis. The formation of a complex between the full-length and v1 hHyal-1 molecules is quite puzzling because the enzyme exists as a monomer both in solution and in the crystal. Conceivably, one may invoke a HyalEGF-like domain swapping that mediates heterodimer formation, however the already extensive interactions between the catalytic and HyalEGF-like domains of the full-length enzyme need to be reconciled.

Clearly, the impact of alternative splicing needs to be further studied. Regardless of the regulatory mechanism, the implication of the available data is that as the bladder cancer progresses, the relative abundance of the full-length hHyal-1 increases compared with the alternative splice variants. This leads to increase in the cellular level of the short-chain HA, promoting cancer growth and proliferation. Strategies that increase the abundance of hHyal-1 splice variants in bladder cancer and reduce the amount of short-chain HA could lead to cancer therapy.

ACKNOWLEDGMENT

We greatly appreciate John Moult's leadership of the Structural Genomics program at CARB. We thank Eugene Melamud, Ethan Zhang, and John Moult for the development of the alternative splicing Web site, Andy Howard for help with synchrotron data collection, and Dr. Joseph L. Johnson for discussion about protein expression in *Drosophila* cells.

REFERENCES

1. Laurent, T. C., and Fraser, J. R. (1992) Hyaluronan, *FASEB J. 6*, 2397−2404.
2. Tammi, M. I., Day, A. J., and Turley, E. A. (2002) Hyaluronan and homeostasis: a balancing act, *J. Biol. Chem. 277*, 4581−4584.

3. Toole, B. P. (2004) Hyaluronan: from extracellular glue to pericellular cue, *Nat. Rev. 4*, 528−539.
4. Stern, R., Asari, A. A., and Sugahara, K. N. (2006) Hyaluronan fragments: an information-rich system, *Eur. J. Cell Biol. 85*, 699−715.
5. Coutinho, P. M., and Henrissat, B. (1999) Carbohydrate-active enzymes: an integrated database approach, in *Recent Advances in Carbohydrate Bioengineering* (Gilbert, H. J., Davies, G., Henrissat B., and Svensson, B. eds, Eds.) pp 3−12, The Royal Society of Chemistry, Cambridge.
6. Stern, R., and Jedrzejas, M. J. (2006) Hyaluronidases: their genomics, structures, and mechanisms of action, *Chem. Rev. 106*, 818−839.
7. Csoka, A. B., Scherer, S. W., and Stern, R. (1999) Expression analysis of six paralogous human hyaluronidase genes clustered on chromosomes 3p21 and 7q31, *Genomics 60*, 356−361.
8. Novak, U., Stylli, S. S., Kaye, A. H., and Lepperdinger, G. (1999) Hyaluronidase-2 overexpression accelerates intracerebral but not subcutaneous tumor formation of murine astrocytoma cells, *Cancer Res. 59*, 6246−6250.
9. Maeda, N., Palmarini, M., Murgia, C., and Fan, H. (2001) Direct transformation of rodent fibroblasts by jaagsiekte sheep retrovirus DNA, *Proc. Natl. Acad. Sci. U.S.A. 98*, 4449−4454.
10. Rai, S. K., Duh, F. M., Vigdorovich, V., Danilkovitch-Miagkova, A., Lerman, M. I., and Miller, A. D. (2001) Candidate tumor suppressor HYAL2 is a glycosylphosphatidylinositol (GPI)-anchored cell-surface receptor for jaagsiekte sheep retrovirus, the envelope protein of which mediates oncogenic transformation, *Proc. Natl. Acad. Sci. U.S.A. 98*, 4443−4448.
11. Csoka, A. B., Frost, G. I., Wong, T., and Stern, R. (1997) Purification and microsequencing of hyaluronidase isozymes from human urine, *FEBS Lett. 417*, 307−310.
12. Aboughalia, A. H. (2006) Elevation of hyaluronidase-1 and soluble intercellular adhesion molecule-1 helps select bladder cancer patients at risk of invasion, *Arch. Med. Res. 37*, 109−116.
13. Lokeshwar, V. B., Cerwinka, W. H., and Lokeshwar, B. L. (2005) HYAL1 hyaluronidase: a molecular determinant of bladder tumor growth and invasion, *Cancer Res. 65*, 2243−2250.
14. Posey, J. T., Soloway, M. S., Ekici, S., Sofer, M., Civantos, F., Duncan, R. C., and Lokeshwar, V. B. (2003) Evaluation of the prognostic potential of hyaluronic acid and hyaluronidase (HYAL1) for prostate cancer, *Cancer Res. 63*, 2638−2644.
15. Triggs-Raine, B., Salo, T. J., Zhang, H., Wicklow, B. A., and Natowicz, M. R. (1999) Mutations in HYAL1, a member of a tandemly distributed multigene family encoding disparate hyaluronidase activities, cause a newly described lysosomal disorder, mucopolysaccharidosis IX, *Proc. Natl. Acad. Sci. U.S.A. 96*, 6296−6300.
16. Jacobson, A., Rahmanian, M., Rubin, K., and Heldin, P. (2002) Expression of hyaluronan synthase 2 or hyaluronidase 1 differentially affect the growth rate of transplantable colon carcinoma cell tumors, *Int. J. Cancer 102*, 212−219.
17. Lin, G., and Stern, R. (2001) Plasma hyaluronidase (Hyal-1) promotes tumor cell cycling, *Cancer Lett. 163*, 95−101.
18. Lokeshwar, V. B., Cerwinka, W. H., Isoyama, T., and Lokeshwar, B. L. (2005) HYAL1 hyaluronidase in prostate cancer: a tumor promoter and suppressor, *Cancer Res. 65*, 7782−7789.
19. Lokeshwar, V. B., Schroeder, G. L., Carey, R. I., Soloway, M. S., and Iida, N. (2002) Regulation of hyaluronidase activity by alternative mRNA splicing, *J. Biol. Chem. 277*, 33654−33663.
20. Lokeshwar, V. B., Estrella, V., Lopez, L., Kramer, M., Gomez, P., Soloway, M. S., and Lokeshwar, B. L. (2006) HYAL1−v1, an alternatively spliced variant of HYAL1 hyaluronidase: a negative regulator of bladder cancer, *Cancer Res. 66*, 11219−11227.
21. Frost, G. I., Csoka, A. B., Wong, T., and Stern, R. (1997) Purification, cloning, and expression of human plasma hyaluronidase, *Biochem. Biophys. Res. Commun. 236*, 10−15.
22. Markovic-Housley, Z., Miglierini, G., Soldatova, L., Rizkallah, P. J., Muller, U., and Schirmer, T. (2000) Crystal structure of hyaluronidase, a major allergen of bee venom, *Structure 8*, 1025−1035.
23. Schultz, J., Copley, R. R., Doerks, T., Ponting, C. P., and Bork, P. (2000) SMART: a web-based tool for the study of genetically mobile domains, *Nucleic Acids Res. 28*, 231−234.
24. Hulo, N., Bairoch, A., Bulliard, V., Cerutti, L., De Castro, E., Langendijk-Genevaux, P. S., Pagni, M., and Sigrist, C. J. (2006) The PROSITE database, *Nucleic Acids Res. 34*, D227−230.
25. Pflugrath, J. W. (1999) The finer things in X-ray diffraction data collection, *Acta Crystallogr., Sect. D: Biol. Crystallogr. 55*, 1718−1725.
26. Storoni, L. C., McCoy, A. J., and Read, R. J. (2004) Likelihood-enhanced fast rotation functions, *Acta Crystallogr., Sect. D: Biol. Crystallogr. 60*, 432−438.
27. Jones, T. A., Zou, J. Y., Cowan, S. W., and Kjeldgaard, G. J. (1991) Improved methods for building protein models in electron density maps and the location of errors in these models, *Acta Crystallogr. A47*, 110−119.
28. Brünger, A. T., Adams, P. D., Clore, G. M., DeLano, W. L., Gros, P., Grosse-Kunstleve, R. W., Jiang, J. S., Kuszewski, J., Nilges, M., Pannu, N. S., Read, R. J., Rice, L. M., Simonson, T., and Warren, G. L. (1998) Crystallography & NMR system: A new software suite for macromolecular structure determination, *Acta Crystallogr., Sect. D: Biol. Crystallogr. 54*, 905−921.
29. Murshudov, G. N., Vagin, A. A., and Dodson, E. J. (1997) Refinement of macromolecular structures by the maximum-likelihood methods, *Acta Crystallogr. D53*, 240−255.
30. Winn, M. D., Isupov, M. N., and Murshudov, G. N. (2001) Use of TLS parameters to model anisotropic displacements in macromolecular refinement, *Acta Crystallogr., Sect. D: Biol. Crystallogr. 57*, 122−133.
31. Holm, L., and Sander, C. (1993) Protein structure comparison by alignment of distance matrices, *J. Mol. Biol. 233*, 123−138.
32. Louie, G. V., Yang, W., Bowman, M. E., and Choe, S. (1997) Crystal structure of the complex of diphtheria toxin with an extracellular fragment of its receptor, *Mol. Cell 1*, 67−78.
33. Jedrzejas, M. J., and Stern, R. (2005) Structures of vertebrate hyaluronidases and their unique enzymatic mechanism of hydrolysis, *Proteins 61*, 227−238.
34. Barinka, C., Sacha, P., Sklenar, J., Man, P., Bezouska, K., Slusher, B. S., and Konvalinka, J. (2004) Identification of the N-glycosylation sites on glutamate carboxypeptidase II necessary for proteolytic activity, *Protein Sci. 13*, 1627−1635.
35. Zhang, F., Murhammer, D. W., and Linhardt, R. J. (2002) Enzyme kinetics and glycan structural characterization of secreted alkaline phosphatase prepared using the baculovirus expression vector system, *Appl. Biochem. Biotechnol. 101*, 197−210.
36. Hofinger, E. S., Spickenreither, M., Oschmann, J., Bernhardt, G., Rudolph, R., and Buschauer, A. (2007) Recombinant human hyaluronidase Hyal-1: insect cells versus E. coli as expression system and identification of low molecular weight inhibitors, *Glycobiology 17*, 444−453.
37. Lokeshwar, V. B., Young, M. J., Goudarzi, G., Iida, N., Yudin, A. I., Cherr, G. N., and Selzer, M. G. (1999) Identification of bladder tumor-derived hyaluronidase: its similarity to HYAL1, *Cancer Res. 59*, 4464−4470.
38. Tews, I., Terwisscha van Scheltinga, A. C., Perrakis, A., Wilson, K. S., and Dijkstra, B. W. (1997) Substrate-Assisted Catalysis Unifies Two Families of Chitinolytic Enzymes, *J. Am. Chem. Soc. 119*, 7954−7959.
39. Iseli, B., Armand, S., Boller, T., Neuhaus, J. M., and Henrissat, B. (1996) Plant chitinases use two different hydrolytic mechanisms, *FEBS Lett. 382*, 186−188.
40. Terwisscha van Scheltinga, A. C., Armand, S., Kalk, K. H., Isogai, A., Henrissat, B., and Dijkstra, B. W. (1995) Stereochemistry of chitin hydrolysis by a plant chitinase/lysozyme and X-ray structure of a complex with allosamidin: evidence for substrate assisted catalysis, *Biochemistry 34*, 15619−15623.
41. Arming, S., Strobl, B., Wechselberger, C., and Kreil, G. (1997) In vitro mutagenesis of PH-20 hyaluronidase from human sperm, *Eur. J. Biochem. 247*, 810−814.
42. Stern, R. (2003) Devising a pathway for hyaluronan catabolism: are we there yet?, *Glycobiology 13*, 105R−115R.
43. Vigdorovich, V., Miller, A. D., and Strong, R. K. (2007) Ability of hyaluronidase-2 to degrade extracellular hyaluronan is not required for its function as a receptor for jaagsiekte sheep retrovirus, *J. Virol. 81*, 3124−3129.
44. Harada, H., and Takahashi, M. (2007) CD44-dependent intracellular and extracellular catabolism of hyaluronic acid by hyaluronidase-1 and -2, *J. Biol. Chem.*, 5597−5607.

45. Harris, R. C., Chung, E., and Coffey, R. J. (2003) EGF receptor ligands, *Exp. Cell Res. 284*, 2−13.
46. Wouters, M. A., Rigoutsos, I., Chu, C. K., Feng, L. L., Sparrow, D. B., and Dunwoodie, S. L. (2005) Evolution of distinct EGF domains with specific functions, *Protein Sci. 14*, 1091−1103.
47. Picot, D., Loll, P. J., and Garavito, R. M. (1994) The X-ray crystal structure of the membrane protein prostaglandin H2 synthase-1, *Nature 367*, 243−249.
48. Hunnicutt, G. R., Primakoff, P., and Myles, D. G. (1996) Sperm surface protein PH-20 is bifunctional: one activity is a hyaluronidase and a second, distinct activity is required in secondary sperm-zona binding, *Biol. Reprod. 55*, 80−86.
49. Bourguignon, L. Y., Singleton, P. A., Diedrich, F., Stern, R., and Gilad, E. (2004) CD44 interaction with Na+-H+ exchanger (NHE1) creates acidic microenvironments leading to hyaluronidase-2 and cathepsin B activation and breast tumor cell invasion, *J. Biol. Chem. 279*, 26991−27007.
50. Junker, N., Latini, S., Petersen, L. N., and Kristjansen, P. E. (2003) Expression and regulation patterns of hyaluronidases in small cell lung cancer and glioma lines, *Oncol. Rep. 10*, 609−616.

BI700382G